Far-Reaching Effects of Okhotsk Sea Ice Area on Sea Surface Heat Flux, Lower Atmosphere, and Ocean Mixed Layer

TOMOHIRO NAKAMURA,[a] YUSUKE TAKAHASHI,[b] TAKUYA NAKANOWATARI,[c] AND HUMIO MITSUDERA[a]

[a] *Pan-Okhotsk Research Center, Institute of Low Temperature Science, Hokkaido University, Sapporo, Hokkaido, Japan*
[b] *Graduate School of Environmental Science, Hokkaido University, Sapporo, Hokkaido, Japan*
[c] *Fisheries Resources Institute, Japan Fisheries Research and Education Agency, Kushiro, Hokkaido, Japan*

(Manuscript received 20 April 2023, in final form 27 September 2023, accepted 13 November 2023)

ABSTRACT: The impact of interannual variations in sea ice area in the Okhotsk Sea was investigated through a composite analysis of years with extensive and limited sea ice areas (referred to as heavy and light ice years, respectively), using atmospheric and oceanic reanalysis data. The comparison of heavy and light ice-year composites in February revealed a substantial decrease in upward surface turbulent heat flux in the Okhotsk Sea (~ -250 W m^{-2}) and a notable increase in a surprisingly extensive region in the western North Pacific (30–120 W m^{-2}), spanning 2300 km from the ice edge. These differences were consistent with the decrease in surface air temperature and specific humidity, suggesting that during heavy ice years, cold and dry air blowing from Siberia to the North Pacific via the Okhotsk Sea undergoes less modification over larger sea ice areas, remaining colder and drier in the North Pacific and thereby enhancing the heat flux. Such advection can be associated with the Asian winter monsoon and migratory cyclones. Cloud cover and surface radiation flux altered consistently with these differences, although longwave and shortwave radiation largely counterbalanced each other. Additionally, the Pacific storm track exhibited variation. In accordance with the heat flux difference, sea surface temperature decreased, and the ocean mixed layer deepened around the subarctic during heavy ice years. These findings suggest that sea ice area in the Okhotsk Sea influences the lower atmosphere and surface ocean in the North Pacific. Such impacts could further affect ocean nutrient circulation, ecosystems, and atmospheric teleconnections.

SIGNIFICANCE STATEMENT: Sea ice cover influences heat exchange between the atmosphere and ocean. Advection of less heated air over larger sea ice areas can enhance heat exchange downwind, and vice versa. We found that this was effective in the Okhotsk Sea, situated along the path of the Asian winter monsoon. Upward surface heat flux increased significantly across a vast region of the North Pacific associated with colder and drier air during years with larger sea ice areas. Additionally, cloud cover, Pacific storm track, sea surface temperature, and ocean mixed layer depth exhibited significant differences associated with sea ice area. These variations could impact ocean heat content, nutrient circulation, and primary production in the North Pacific, and atmospheric circulation in North America and Europe.

KEYWORDS: Sea ice; Atmosphere–ocean interaction; Oceanic mixed layer; Heat budgets/fluxes; Surface temperature; Interannual variability

1. Introduction

The Okhotsk Sea is a seasonal sea ice region with substantial interannual variability (Parkinson and Cavalieri 2008). The maximum sea ice extent ranges from 70×10^4 to 152×10^4 km^2 (Japan Meteorological Agency 2023). Such a high range of interannual variation in sea ice area (SIA) in the Okhotsk Sea shows significant correlations with lower atmospheric circulation (Fang and Wallace 1994, 1998; Tachibana et al. 1996; Yamazaki 2000; Ohshima et al. 2006; Ogi and Tachibana 2006; Yamamoto et al. 2006; Ukita et al. 2007; Liu et al. 2007; Sasaki et al. 2007; Nakanowatari et al. 2010) and sea surface temperature (SST; Ogi and Tachibana 2006; Sasaki et al. 2007; Nakanowatari et al. 2010). Previous studies thus attributed the SIA variation in the Okhotsk Sea to the interannual variations of the surrounding atmosphere and ocean.

Conversely, SIA variations modify the surface heat flux, thereby affecting the atmosphere and ocean. Sea ice reduces surface turbulent heat flux due to its heat-insulating effect (Inoue et al. 2003). This effect causes prominent variations in heat flux in the central Okhotsk Sea, where sea ice cover variability is high (Ohshima et al. 2006; Liu et al. 2007; Iwamoto 2007). Honda et al. (1999) suggested that the change in heat flux in the Okhotsk Sea can generate a stationary Rossby wave train that transports the effects of SIA variations to North America. Screen (2017) highlighted that the Okhotsk Sea is one of the regions that will have the strongest responses to future sea ice decrease in winter, which would further affect the atmospheric circulation over the North Atlantic and Europe as well as North America. Furthermore, such changes in surface heat flux may affect the development of oceanic mixed layer in winter, thereby affecting ocean material circulation.

In addition to the central Okhotsk Sea, which has high sea ice variability, it is likely that surface turbulent heat flux also alters in its downwind through atmospheric advection, since the Okhotsk Sea is located in the Asian winter monsoon

Corresponding author: Tomohiro Nakamura, nakamura@lowtem.hokudai.ac.jp

DOI: 10.1175/JCLI-D-23-0239.1

region. Deser et al. (2010) indicated the importance of atmospheric advection from the Arctic Ocean to the surrounding continents in the responses to projected Arctic sea ice loss. In the case of the Okhotsk Sea, monsoon winds blow from Siberia to the North Pacific via the Okhotsk Sea; thus, we may expect that a larger (smaller) SIA would heat cold air from Siberia less (more) while moving through the Okhotsk Sea, and its advection would modify surface turbulent heat flux downwind in the North Pacific.

Further, it is also likely that changes in surface turbulent heat flux would affect clouds and radiation. Since surface sensible and latent heat fluxes correspond to heat and moisture supplies from the ocean, changes in these fluxes would impact cloud formation and, consequently, radiation flux. Alterations in radiation flux would also modify the surface heat flux. Additionally, as the Okhotsk Sea is adjacent to or partially overlapping the Pacific storm track (Lau 1988), its relation with the Okhotsk Sea SIA is intriguing as it could in turn affect heat flux.

However, the effects of SIA variations in the Okhotsk Sea on surface heat flux and the ocean are not well understood. In particular, as far as we are aware, realistic impacts on surface heat flux in the North Pacific, surface radiation flux, the storm track, and the ocean mixed layer have not been investigated using observations or reanalysis. Although many atmospheric general circulation model experiments were recently conducted to study responses to sea ice loss in and around the Arctic, its impact on surface heat flux over the ocean have not been explored. In addition, the responses were shown to differ between models and reanalyses (Smith et al. 2022); differences were also indicated in the responses to simultaneous sea ice loss around the Arctic and the sum of those to regional sea ice losses (Screen 2017). Therefore, we attempted to characterize the impact of the Okhotsk Sea SIA variation, focusing on the downwind region of the North Pacific, by conducting a composite analysis of heavy and light ice years using atmospheric and oceanic reanalyses.

In the following, section 2 describes the data and methods used in the study. Changes in sea surface turbulent heat flux and their primary causes are discussed in section 3. We present the alterations in cloud cover and radiation flux in section 4, those in the storm track in section 5, and those in the ocean mixed layer in section 6. The results are summarized and discussed in section 7.

2. Data and methods

a. Data

The primary data analyzed were the Japanese 55-year Reanalysis (JRA-55; Kobayashi et al. 2015) for the atmosphere and the four-dimensional variational ocean reanalysis for the western North Pacific over 30 years (FORA-WNP30; Usui et al. 2017) for the ocean. Additionally, the sea ice extent data published by the JMA were utilized for a comparison with the JRA-55 sea ice data, although the conclusions of this study are essentially based only on the atmospheric and oceanic reanalyses.

Atmospheric and sea ice data comprised the 1.25° latitude/longitude grid version of JRA-55. We used 6-hourly analysis field parameters when available (wind, temperature, specific humidity, and pressure); in their absence, we used 3-hourly forecast field parameters (sensible and latent heat fluxes, radiation flux, and cloud cover). The JRA-55 sea ice cover was integrated to calculate SIA, where JRA-55 regards a region with sea ice concentration above 0.55 as a sea ice area. The results were compared with the JMA sea ice extent data (2016). JMA derived the sea ice extent data from satellite and other observations adopting a threshold of 0.11 sea ice concentration. These data span from 15 December 1970 to the present, at 5-day intervals. Interannual variations of the JRA-55 SIA differed significantly before 1980 from those of JMA sea ice extent. After 1979, the variations were consistent with both the JMA sea ice extent and the National Snow and Ice Data Center dataset reported by Parkinson and Cavalieri (2008). Thus, the atmospheric data were analyzed for the period of 1980–2016.

The ocean reanalysis, FORA-WNP30, uses JRA-55 products for atmospheric forcing, ensuring consistency between atmospheric and ocean data. FORA-WNP30 has a horizontal resolution of 1/10° × 1/10° and 54 vertical levels. The analysis period spanned 1982–2015, which was the longest available data period at the time of our analysis. Potential temperature and salinity were used to calculate the potential density and mixed layer depth (MLD). MLD was defined here as the depth at which potential density exceeds the surface value by 0.03 kg m^{-3} (Thomson and Fine 2003). Note that if potential density is vertically uniform, both potential temperature and salinity are also uniform, and hence such a layer can be regarded as a mixed layer (unless the contributions of potential temperature and salinity to density stratification cancel out perfectly, which is an exceptionally rare case). We also tested a threshold of 0.125 kg m^{-3} (Levitus 1982) and obtained qualitatively similar results.

b. Composite analysis: Heavy and light ice years

SIA in the Okhotsk Sea typically reaches its maximum between February and March, with yearly variations. Nevertheless, the interannual variations in SIA are qualitatively similar among the maximum, February mean, and March mean SIA (Fig. 1a). To reduce the influence of seasonal progression, we analyzed the monthly mean fields for February and March. Analyzing a duration (e.g., 30 days) centered on the days of the SIA maximum would yield different dates each year, and the results would be influenced by differences due to seasonal progression. The February and March means yielded qualitatively similar results, although the February mean results exhibited stronger responses as they better represent winter climate characterized by lower air temperatures and stronger air–sea heat exchange. Thus, we present only the February mean results.

We constructed composites of heavy and light ice years and examined their differences. Heavy and light ice years are defined as those with a monthly mean SIA greater or less than one standard deviation from the average, respectively (Fig. 1a). There were four heavy and seven light ice years with nine

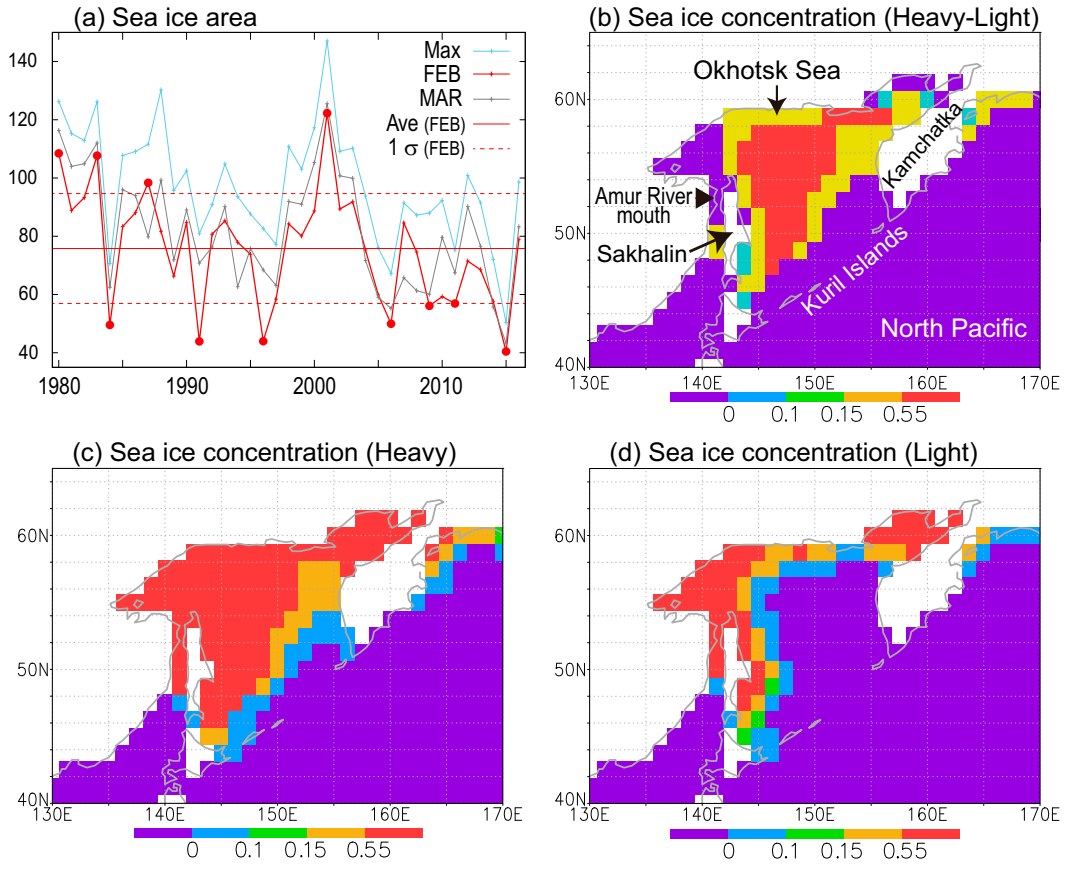

FIG. 1. (a) Interannual variation of sea ice area in the Okhotsk Sea (10^4 km^2). Also shown are composites of sea ice concentration in February: (b) the difference between the heavy and light ice years and the (c) heavy and (d) light ice years. Heavy and light ice years in February are denoted by circles in (a), where the maximum (blue), February mean (red), and March mean (gray) SIA are plotted.

degrees of freedom for the atmospheric reanalysis, and three heavy ice years with eight degrees of freedom for the oceanic reanalysis because of the shorter analysis period. Statistical significance was assessed using a *t* test. Light ice years have been more frequent in recent years (Fig. 1a), potentially due to global warming. We estimated the effect of this uneven occurrence by conducting the same analysis but with data before 2002 and obtained qualitatively similar results.

Before analyzing the atmosphere and ocean, the composites of sea ice concentration in the heavy and light ice years and their differences are presented in Figs. 1b–d. Sea ice covered most of the Okhotsk Sea during the heavy ice years, excluding a region near the Kuril Islands (Fig. 1c), whereas it was limited to the northern and western parts during the light ice years (Fig. 1d). The central Okhotsk Sea showed substantial differences (Fig. 1b) and is hereafter referred to as the sea ice variability region.

3. Difference in sea surface turbulent heat flux and surface atmosphere

The substantial difference in sea ice concentration between the heavy and light ice years (Fig. 1b) would modify the surface turbulent heat flux. This section examines the differences in surface turbulent heat flux and explores the possibility that their effects can be spread to the North Pacific by advection.

a. Sensible and latent heat fluxes, temperature, specific humidity, and pressure

Figures 2a and 2b show the differences in sensible and latent heat fluxes (heavy minus light ice years), respectively. Both heat fluxes were negative (downward) in the sea ice variability region and positive (upward) around the Kuril Islands, extending southeastward to eastward to 175°E. When combined, statistically significant negative and positive anomalies reached −250 and 30–150 W m^{-2}, respectively. Figures 2c and 2d show that negative anomalies in surface air temperature (SAT) and specific humidity (SH) spread from the sea ice variability region to the North Pacific, reaching 165°W. The SAT difference reached 3–4 K in the North Pacific, which was considerably larger than the interannual SST variability in the corresponding region, suggesting a stronger influence on interannual variations in surface heat flux than the SST variations in this region.

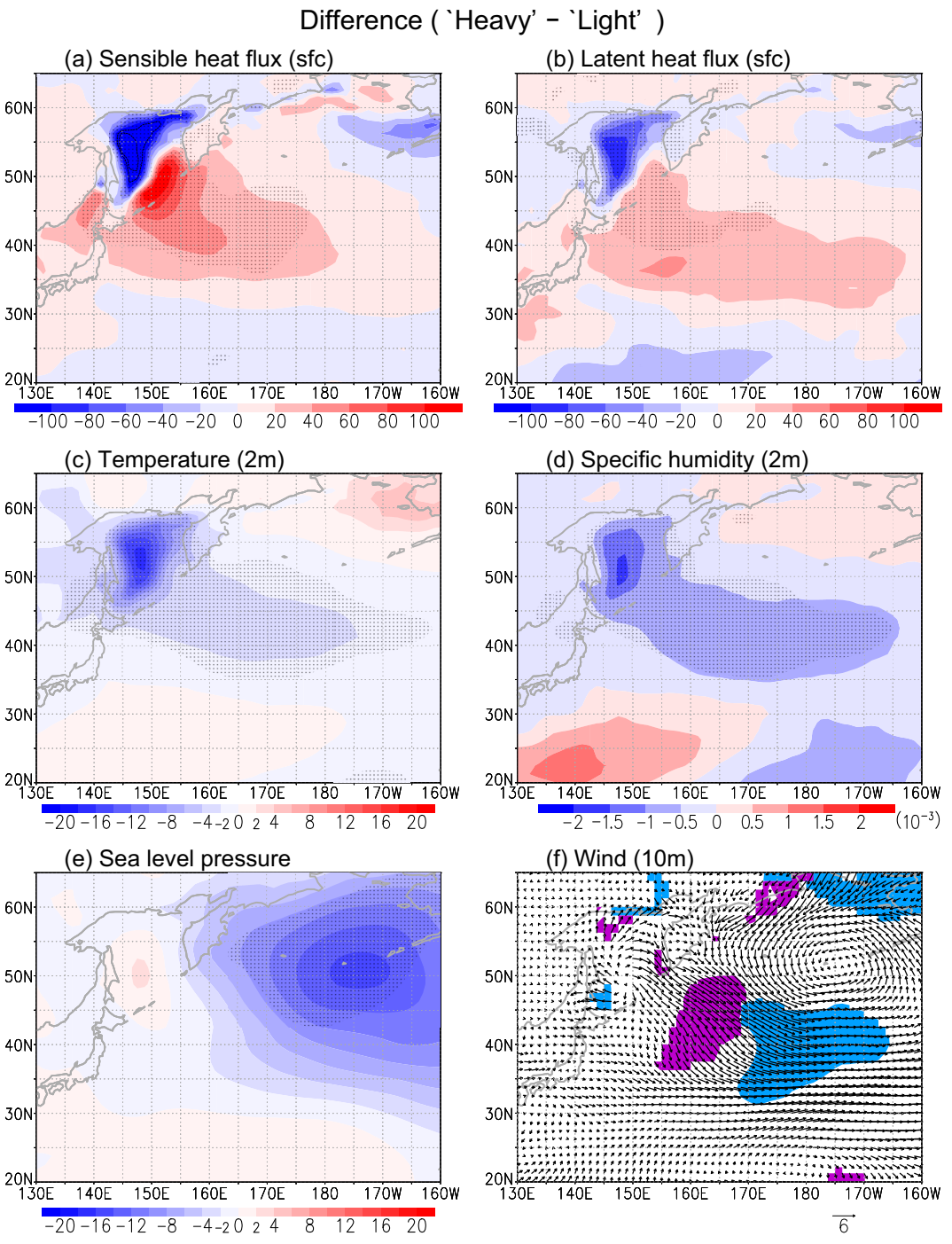

FIG. 2. Difference in surface heat flux and surface atmosphere (heavy − light ice years) in February: (a) sensible and (b) latent heat fluxes (positive upward; W m^{-2}), (c) air temperature (2 m; K), (d) specific humidity (2 m; kg kg^{-1}), (e) sea level pressure (hPa), and (f) wind (10 m; m s^{-1}). Positive anomalies indicate increased values in the heavy ice years when compared with those in the light ice years. Stippling signifies differences at 95% confidence level. In (a), contours are −120 and −140 W m^{-2}. In (f), blue and purple shading represent 95% confidence levels for the zonal and meridional components, respectively. The arrow below the panel indicates the scale of the wind velocity vectors.

Comparisons of the differences in the Okhotsk Sea showed that the distributions of the negative anomalies of sensible and latent heat fluxes and those of strong negative anomalies of SAT and SH (Figs. 2a–d) match the distribution of the difference in sea ice concentration (Fig. 1b), suggesting the effects of the SIA difference. Thus, it is likely that the heat insulating effect of sea ice causes the negative sensible and latent heat flux anomalies (i.e., decrease in heavy ice years), which in turn decrease SAT and SH in the sea ice variability region. Conversely, although a decrease in SAT and SH may increase SIA, it is unlikely in the present case, because the differences in SAT and SH were insignificant upwind of the Okhotsk Sea with their peaks located in the sea ice variability region (Figs. 2c,d). It is also unlikely that the decreases in SAT and SH reduced the turbulent heat fluxes, as such decreases over a warmer sea act to increase the turbulent heat fluxes.

In the downwind of the sea ice variability region, the negative SAT and SH anomalies extended roughly along the climatological surface winds in February (omitted) and were located in regions similar to the positive heat flux anomalies (Figs. 2a–d). This suggests that negative SAT and SH anomalies are advected from the Okhotsk Sea to the North Pacific, increasing the heat flux in the latter region. Similar changes in SAT and SH occurred at 925 and 850 hPa, with downwind shifts of the peaks with increasing height (not shown), supporting the effect of advection from the sea ice variability region. Note that the converse is unlikely, because positive heat flux acts to increase SAT and SH. Advection from regions other than the Okhotsk Sea is also unlikely to contribute significantly to the positive heat flux anomaly, as almost no significant differences were found in other regions. The above arguments suggest that in heavy ice years, cold and dry air from Siberia is advected to the North Pacific with less modification in the Okhotsk Sea because of larger SIA, decreasing SAT and SH and increasing the turbulent heat fluxes downwind in the North Pacific.

The difference in sea level pressure (SLP) indicates that the Aleutian low was stronger during the heavy-ice years, with a slight eastward shift (Fig. 2e). Although a positive but statistically insignificant SLP anomaly in the Okhotsk Sea suggests the SIA effects, which is qualitatively consistent with the results of Honda et al. (1999), a wave train pattern originating from the Okhotsk Sea was not discernible. This suggests that the SLP difference would be affected mainly by interannual variations in the background atmosphere, which caused the SIA variations. Associated with the SLP difference, northerly and westerly winds significantly strengthened along the Aleutian low (Fig. 2f). This wind difference could have contributed to the spread of colder and drier air during the heavy ice years.

It should be emphasized that the above analysis did not isolate the effects of the SIA variations. Interannual variations in the background atmosphere may also affect the differences in heat fluxes. Thus, we attempted to assess the contribution of the SIA variation in the next subsection.

b. *Contributions to turbulent heat flux difference*

To assess the contributions of the SIA differences to the positive turbulent heat flux anomalies (Fig. 2), we first compared the contributions of the differences in SAT, SH, and wind speed to the positive heat flux anomalies. The former two were likely affected by the SIA difference. We then attempted to estimate the proportions of the positive heat flux anomalies attributable to the SIA difference.

First, we decomposed the turbulent heat flux terms using the bulk equations as follows:

$$\Delta\varphi = \varphi_{\mathrm{HIY}} - \varphi_{\mathrm{LIY}},$$

$$\Delta Q_s = \rho C_p C_H [V_{\mathrm{LIY}}(\Delta T_o - \Delta T_a) + \Delta V(T_{o\mathrm{LIY}} - T_{a\mathrm{LIY}}) + \Delta V(\Delta T_o - \Delta T_a)], \text{ and} \quad (1)$$

$$\Delta Q_l = \rho L C_E [V_{\mathrm{LIY}}(\Delta q_o - \Delta q_a) + \Delta V(q_{o\mathrm{LIY}} - q_{a\mathrm{LIY}}) + \Delta V(\Delta q_o - \Delta q_a)]. \quad (2)$$

Here, Δ represents the difference between the heavy and light ice years (subscripts HIY and LIY denote the composite of heavy and light ice years), φ is an arbitrary variable, Q_s and Q_l represent sensible and latent heat fluxes, C_H and C_E are bulk transfer coefficients for sensible and latent heat, L is the latent heat of evaporation or sublimation, C_p denotes the specific heat at constant pressure, ρ is the density of air, V is the wind speed, and T and q are temperature and specific humidity, with subscripts o and a indicating ocean and atmosphere, respectively. For simplicity C_H, C_E, L, C_p, and ρ were set as constant [the first two values corresponding to neutral stability based on Kondo (1975)], and the same formulas on both open water and sea ice were used following Ohshima et al. (2003) and Nihashi et al. (2012). The flux differences calculated using these equations (Figs. 3a,d) were similar to those of JRA-55 (Figs. 2a,b), suggesting that the simplified bulk equations are sufficient to specify the main contributions. The first terms in Eqs. (1) and (2) represent the contributions of temperature and SH differences, and the second terms represent those of wind speed difference. The products of the differences (the third terms) were relatively small and thus omitted. In fact, the ratio of the third term to the first term becomes $\Delta V/V_{\mathrm{LIY}}$ in both equations, and it was $< 10\%$ in most of the North Pacific and 20%–30% around the sea ice variability region.

The contributions of the temperature and SH differences (Figs. 3b,e) resembled the sensible and latent heat flux differences (Figs. 3a,d), respectively, in terms of both magnitude and distribution. The differences were much larger in the atmosphere (ΔT_a and Δq_a) than in the ocean (ΔT_o and Δq_o, respectively), except over the sea ice variability region, where the differences were larger in the ocean (i.e., difference between water and ice surfaces). The results suggest that the differences in SAT and SH were the main causes of the positive turbulent heat flux anomalies outside the sea ice variability region, while the differences between seawater and ice were the main causes of the negative heat flux anomalies in the sea ice variability region. This supports the importance of the heat insulating effect of sea ice and cold and dry advection.

The wind speed difference (Figs. 3c,f) contributed less to the sensible and latent heat flux differences. Nevertheless, its

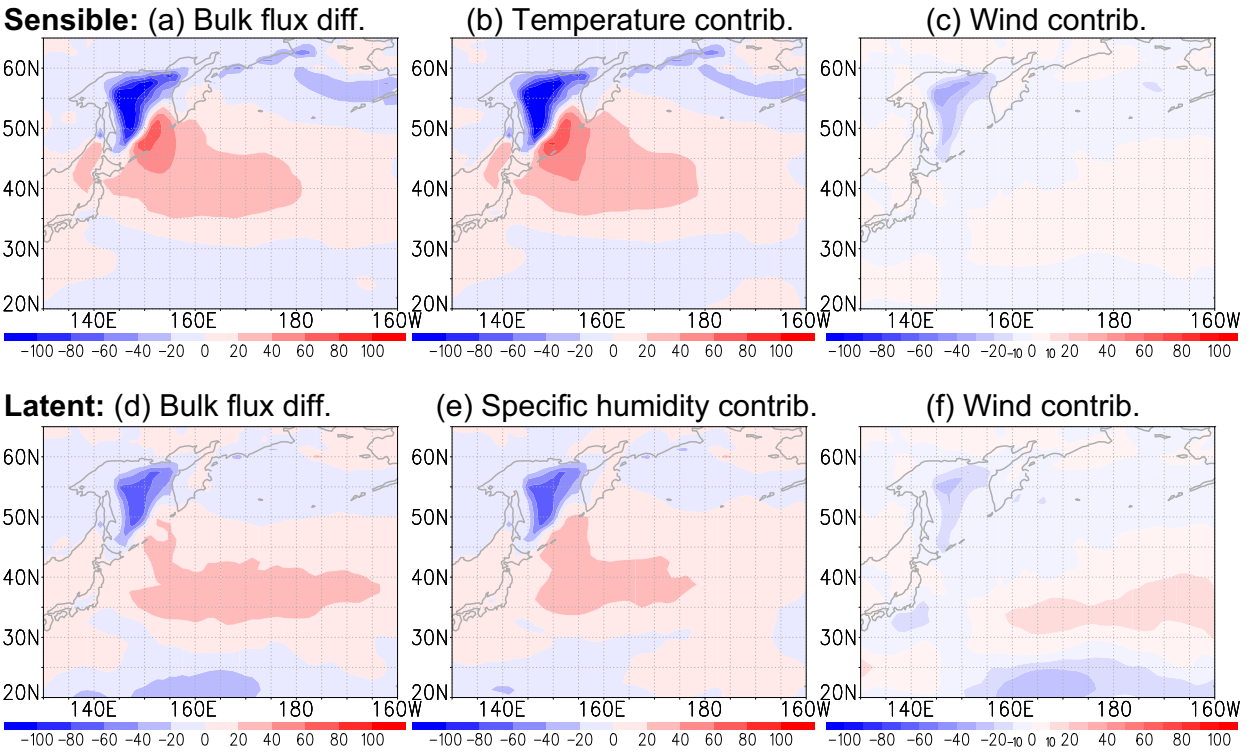

FIG. 3. Contributions to differences in (a)–(c) sensible and (d)–(f) latent surface heat fluxes (positive upward; W m^{-2}) in February, estimated using bulk Eqs. (1) and (2), for (left) total bulk fluxes, with contributions from (center) air temperature [in (b)] and specific humidity [in (e)] and (right) scalar wind. Positive values indicate a relative increase during the heavy ice years.

contribution to the latter was similar in magnitude to that of the SH difference over a band extending eastward from 165°E along ~35°N. This is one of the reasons why the positive anomaly of latent heat flux extended farther east than that of sensible heat flux. However, the change in wind in such a distant region may be largely associated with changes in the background atmosphere and the Pacific storm track (discussed in section 5). Note that even without changes in wind, temperature or SH changes can alter advection effects, and thus the small change in wind speed does not contradict with the importance of advection.

Second, encouraged by the dominance of the temperature and SH contributions, we attempted to estimate the extent to which the positive heat flux anomalies were caused by the SIA difference. For this estimation, considering that there was no significant difference in SAT and SH both upwind of the Okhotsk Sea and sufficiently downwind in the North Pacific, we assumed that the differences between the upwind and sufficiently downwind regions in temperature and SH of the lower atmosphere are approximately the same in heavy and light ice years (more precisely, the heat and water content of the layer that affects the surface turbulent heat flux). In other words, during the course of advection of the cold and dry air from Siberia to the North Pacific via the Okhotsk Sea, the total amounts of heat and water vapor supplied to the atmosphere are assumed to be the same for both heavy and light ice years, but their location shifts downwind in heavy ice years because of larger SIA, such that the total negative and positive heat flux anomalies become equal. This means that an amount of the positive heat flux anomaly equal to the total negative heat flux anomaly should be directly attributed to the SIA change, while the remainder could be attributed to other factors. Note that this assumption is a relatively rough estimate because heat flux depends nonlinearly on temperature; if an air mass with the same SAT is exposed to a higher SST in the south, it should result in a larger heat exchange. Additionally, the increase in SAT due to surface heat flux also depends on atmospheric convection (i.e., vertical heat distribution), which may alter subsequent heat exchange downwind.

Based on the above assumption, we compared the area integrals of the positive and negative heat flux anomalies within 95% confidence level (i.e., dotted areas in Fig. 2). For sensible and latent heat fluxes, the integrated negative fluxes were approximately half the amount and the same amount of the integrated positive fluxes, respectively. Combining both fluxes yielded ~60% of the integrated positive flux. That is, ~60% of the heat flux increase downwind of the sea ice variability region can be explained by the heat flux decrease due to the SIA increase. This simple estimate suggests that the SIA change is the primary cause of the widely distributed positive turbulent heat flux anomaly.

c. *Cold-advection events*

Although the SAT and SH differences in the North Pacific roughly followed climatological winds, the regions of these

differences overlap with the Pacific storm track and hence experience migratory cyclones. Such strong short-term disturbances would also contribute to the advection of cold and dry air from the Okhotsk Sea, as well as the climatological mean winds. Moreover, the Lagrangian trajectories may differ from an Eulerian mean wind field in the presence of strong disturbances. Thus, we made a composite of cold-advection events associated with short-term disturbances in February to examine the surface heat flux caused by such disturbances and estimate the extent of the winds blowing from the Okhotsk Sea.

The events were defined as periods during which the area-averaged temperature at 2 m, 925 hPa, and 850 hPa were lower than 1 standard deviation from the February mean in each year, using 6-hourly analysis fields for consistency (although 3-hourly forecast fields yielded similar results). The area used for averaging was 40°–45°N, 155°–170°E southeast of the Okhotsk Sea, which exhibited significant cold, dry, and upward turbulent heat flux anomalies (Figs. 2a–d). These cold-advection events occurred two to four times (average 2.3 times) in February each year, roughly corresponding to the stronger half of migratory cyclones. The total numbers of occurrences were 10 and 15 for the heavy and light ice years, respectively, which the degree of freedom was based on. The average duration was 25 h, which was relatively short as only the vicinities of the peaks were extracted. The composites of these events were then calculated for the heavy and light ice years (Fig. 4). The cold-advection events correspond to peaks of northwesterly winds associated with strong migratory cyclones located east of the Okhotsk Sea, which was seen as cyclonic winds centered around 50°N, 170°E (Fig. 4e) although blurred because of composition. To reduce the influence of differences in the background atmosphere between years, we subtracted the February mean of the corresponding year before making the composites, and then calculated the composites of these differences for the heavy and light ice years.

In the heavy ice years, the cold advection generated strong positive upward sensible and latent heat fluxes from the ice edge to the subtropics (Figs. 4a,c), with maximum values exceeding 250 and 300 W m^{-2}, respectively. The effects of cold advection from the sea ice region were particularly evident when the monthly mean was subtracted (contours in Figs. 4a,c). Positive anomalies of both sensible and latent heat fluxes extended southeast from the ice edge to the Kuroshio Extension, with maximum values still exceeding 100 and 80 W m^{-2}, respectively (Figs. 4a,c), including most of the regions of significant positive heat flux anomalies (Figs. 2a,b). The winds blowing from the Okhotsk Sea reached these large flux regions (Fig. 4e), supporting that the air influenced by sea ice cover can span such a broad region, thereby enhancing the heat flux.

These positive heat flux anomalies (Figs. 4a,c) appeared somewhat different from those in Figs. 2a and 2b in a way that they extended more meridionally, reaching farther south, and differed notably between sensible and latent heat fluxes. The former difference can be associated with higher wind speed and stronger meridional wind component of migratory cyclones compared with the climatological winds, resulting in stronger transport of a cold and dry air southeastward (Fig. 4e). The peak sensible heat flux occurred near the ice edge, whereas the peak latent heat flux occurred near the Kuroshio Extension, and the positive latent heat flux anomaly extends south of 25°N, farther south than the sensible heat flux anomaly. These are attributed to the ratio of sensible heat flux to latent heat flux (i.e., Bowen ratio) that generally increases with decreasing temperature over the oceans, and vice versa. In the present case, the ratio is high around the ice edge because of low SST, whereas it is low in the subtropics because of high SST. Accordingly, latent heat flux increased with decreasing latitude, peaking around the Kuroshio Extension; thus, its anomaly reached farther south than the sensible heat flux anomaly. Nevertheless, since it takes nearly 3 days for an air mass to travel from the Okhotsk Sea to 20°N with a wind speed of 10 m s^{-1}, the anomaly south of 25°N might not be associated with air masses from the Okhotsk Sea, although the wind composite suggests that relatively cold and dry air could reach this point (Fig. 4e).

In the light ice years, although the basic features during cold-advection events were similar to those in the heavy ice years (Figs. 4b,d,f), heat fluxes were smaller and began to increase in the northern Okhotsk Sea, reflecting the smaller SIA. Wind from east of the Kamchatka Peninsula was also significant (Fig. 4f). This suggests that cold advection from the western Bering Sea in the light ice years weakened the effects of the SIA variations in the Okhotsk Sea on the North Pacific, particularly in the eastern part of the positive heat flux anomalies (Figs. 2a,b). In addition, heat flux anomalies were not significant near the ice edge (northern to western Okhotsk Sea). This indicates that the region used to define cold-advection events here may be located too east compared with the sea ice distribution in light ice years (i.e., the present definition is suited for heavy ice years), and the heat flux distribution would be altered by shifting the position of the region used for definition.

4. Cloud cover and radiation flux

Significant differences in heat and water vapor supply from the ocean (Figs. 2a,b) imply potential variations in cloud cover and radiation heat fluxes. This section investigates this possibility.

a. Cloud cover

Low-level cloud cover decreased substantially over the sea ice variability region in the Okhotsk Sea during the heavy ice years in February (Fig. 5a). This corresponds to a shift in the cloud formation region due to sea ice cover, particularly cloud streets (or cloud bands). Cloud streets, which are associated with horizontal roll vortices, develop when cold and dry continental air (e.g., Siberia) blows over much warmer water (Okhotsk Sea) in winter. However, sea ice cover prevents cloud streets formation by reducing heat and water vapor supply, shifting their formation region downwind of the sea ice cover. In the heavy ice years, the cloud formation region moved downwind (southeast) of the sea ice variability region, resulting in the negative anomaly there.

Middle- and high-level cloud cover also decreased significantly in the Okhotsk Sea, with peaks shifting downwind (southeast) with increasing height (Figs. 5b,c). This is consistent with the downwind movement of the cloud streets that deepen and change into open-cell mesoscale convection. During the light ice

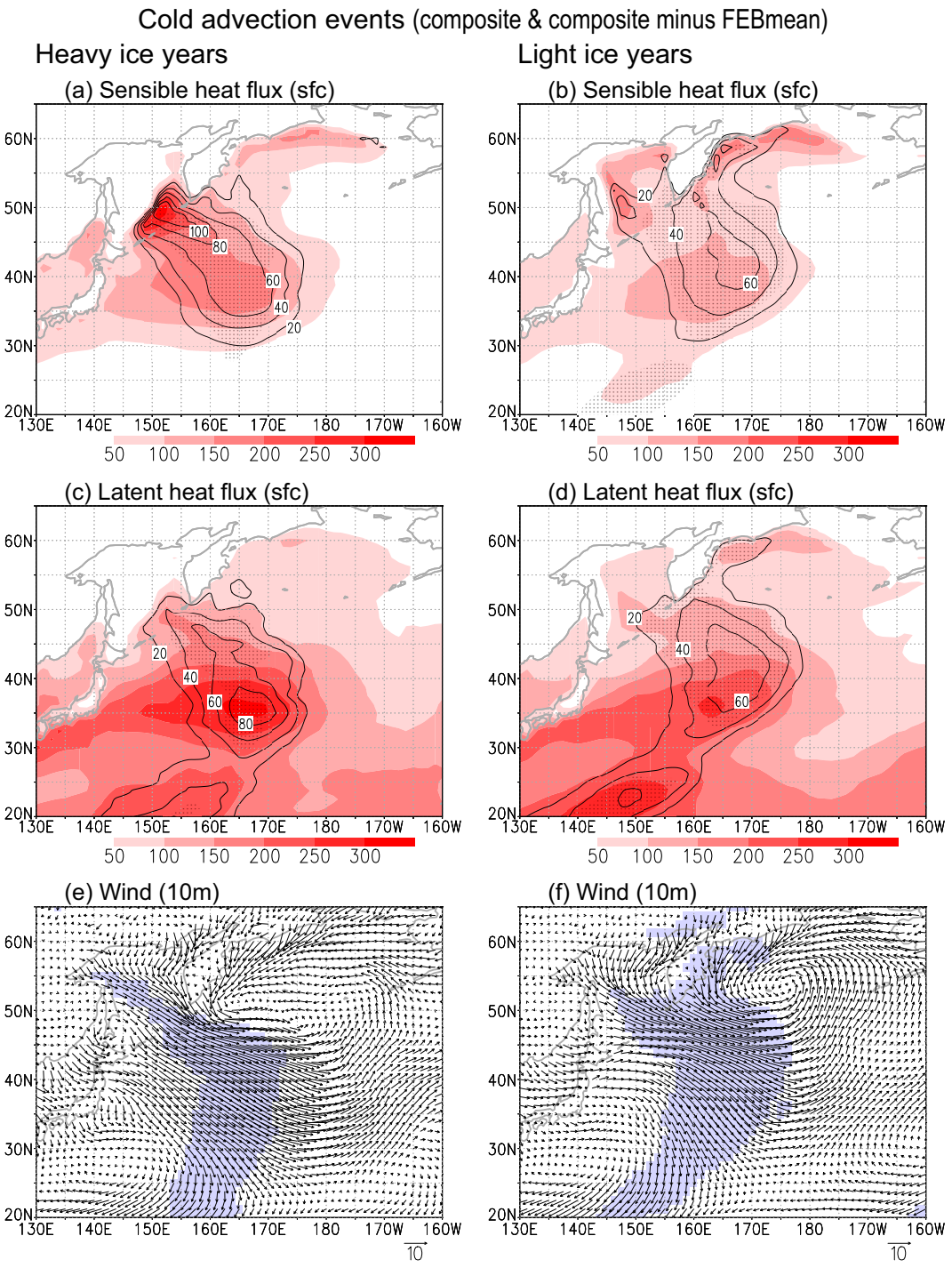

FIG. 4. Composite of the cold-advection events in (left) heavy and (right) light ice years during February for (a),(b) sensible and (c),(d) latent surface heat fluxes (positive upward; W m^{-2}), and (e),(f) surface wind (10 m; m s^{-1}). Shading and contours in (a)–(d) indicate the respective heat flux composites and anomalies, where anomalies represent values after subtracting the February mean of the corresponding years. Stippling denotes anomalies at 95% confidence level. Blue shading in (e) and (f) denotes northerly and westerly wind anomalies with 95% confidence level.

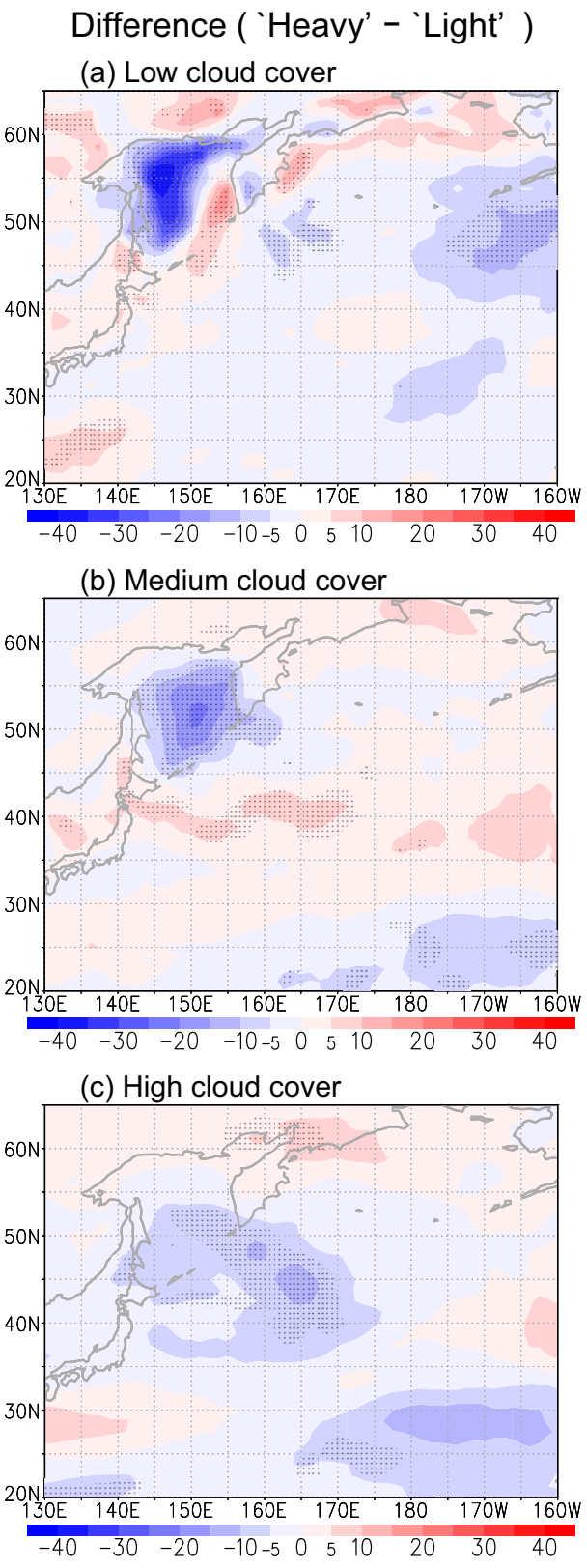

FIG. 5. Difference in cloud cover (%) at (a) low, (b) middle, and (c) high levels in February. Positive values indicate a relative increase in cloud cover during the heavy ice years. Stippling denotes differences at 95% confidence level.

years, cloud streets formed more upwind and developed to higher levels while moving downwind, resulting in the downwind shift of the negative anomalies with increasing height. During the heavy ice years, cloud streets formed more downwind and remained at lower levels when compared at the same location, which is consistent with significant positive anomalies of low- and middle-level cloud cover in the downwind of the negative anomalies (Figs. 5a,b). As for high-level cloud cover, the downwind of the negative anomaly was in the subtropics and the storm track, leading to an absence of significant positive anomaly. Similarly, an increase in middle-level clouds around 40°N could be also related to changes in the storm track.

b. *Longwave radiation flux*

The changes in cloud cover (Fig. 5) would influence the downward longwave radiation at the surface, which is mostly determined by cloud, temperature, and water vapor. Further, the wider and cold ice surface in heavy ice years would reduce the upward longwave radiation. Thus, longwave radiation flux was examined.

The net upward longwave flux at the surface decreased significantly over the sea ice variability region in the Okhotsk Sea, whereas it increased significantly from around the Kuril Islands to the western subarctic Pacific during the heavy ice years (Fig. 6a). The magnitude of these differences ranged from 10 to 30 W m^{-2}. To consider the reason for these changes, the difference in the downward longwave flux is presented in Fig. 6c. The downward longwave flux decreased substantially over the Okhotsk Sea and significantly in a broad region in the North Pacific. Despite this substantial decrease, the net upward longwave flux decreased in the sea ice variability region, indicating that the decrease in downward flux was still smaller than decrease in the upward longwave flux due to the cold ice surface. In other regions, a significant increase in the net upward flux was mostly associated with a decrease in the downward flux. A change in the upward flux due to an SST difference was considerably smaller (e.g., an SST difference of 2 K results in a difference of <3% in upward longwave radiation).

When looked at closely, although the decrease in the downward flux was consistent with the cloud cover reduction in the Okhotsk Sea, it spread more widely in the North Pacific (Figs. 6c and 5), which could not be explained by cloud cover alone. Indeed, the clear-sky downward longwave flux decreased significantly in a broad region, such that both distribution and magnitude were similar to those of the downward flux in the North Pacific (Figs. 6e,c). This suggests the importance of temperature and water vapor, major factors for longwave radiation besides clouds, and is consistent with the similar distributions of the negative anomaly in the clear-sky downward longwave flux (Fig. 6e) and the negative SAT and SH anomalies (Figs. 2c,d). To estimate the effect of SH on longwave radiation, the effective water vapor amount for longwave (e.g., Katayama 1966)

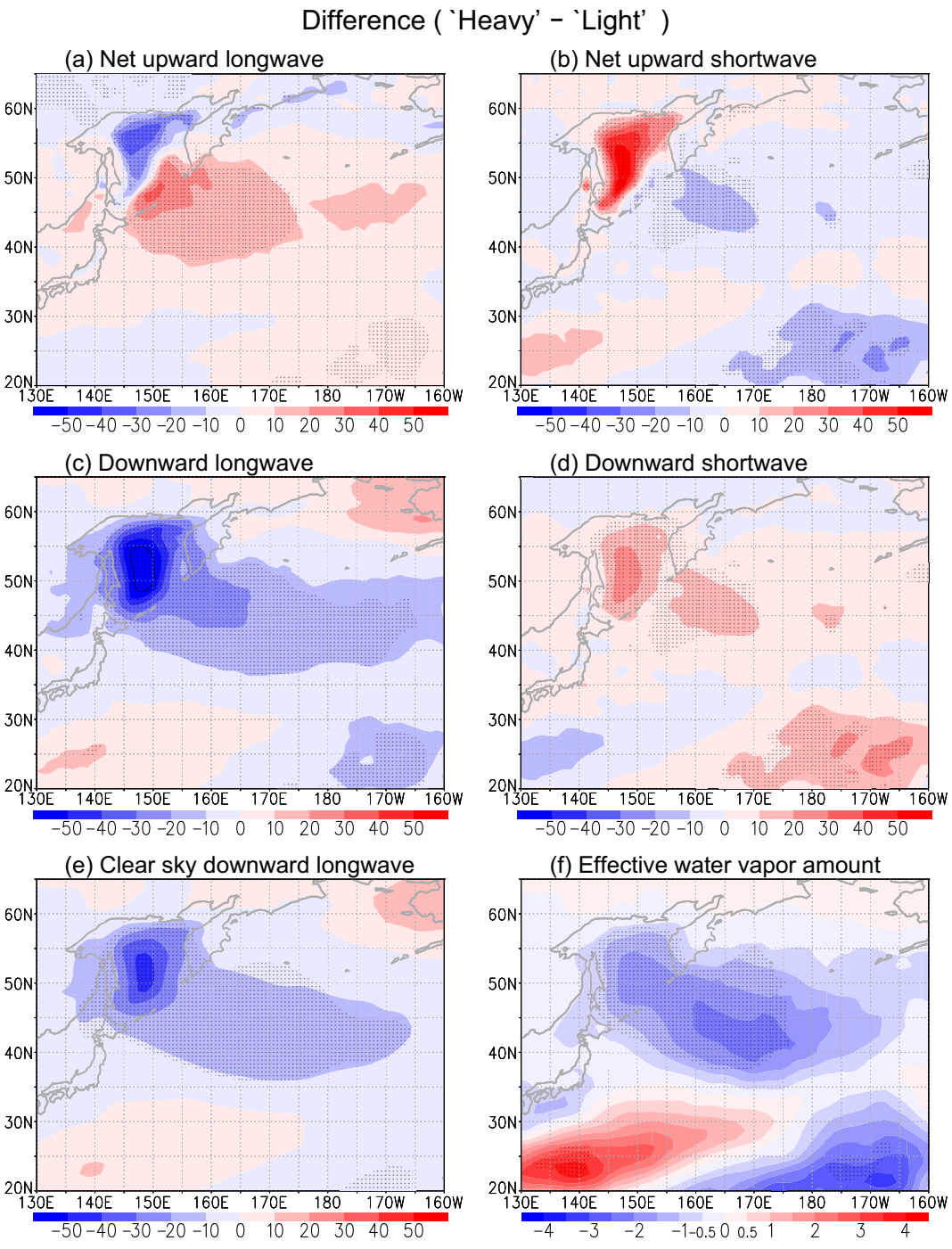

FIG. 6. Difference in surface radiation fluxes (W m^{-2}) and effective water vapor amount (kg m^{-2}) in February: net upward (a) longwave and (b) shortwave and downward (c) longwave and (d) shortwave radiation fluxes, (e) clear-sky downward longwave radiation flux, and (f) effective water vapor amount. Positive values indicate a relative increase in the heavy ice years. Stippling denotes differences at 95% confidence level. The contour in (c) is -60 W m^{-2}.

was calculated (Fig. 6f), as water vapor needs pressure correction. It decreased significantly in a similar region but with the peak in the North Pacific, supporting the importance of water vapor difference in downward longwave flux difference in the Pacific. We estimated the radiation flux change caused by differences in temperature and the effective water vapor amount following Kondo (2000). The estimated change accounted for the decrease in the clear-sky downward longwave flux around the Kuril Islands and the western subarctic Pacific, where changes in temperature

and water vapor contributed approximately 60% and 40%, respectively. These results suggest that the reduction in cloud cover, air temperature, and water vapor during heavy ice years results in a decrease in the downward longwave flux at the surface compared with light ice years.

c. *Shortwave radiation flux*

Variations in cloud cover and sea ice extent should also influence the downward and upward shortwave radiation flux through a sun-shading effect and changes in albedo, respectively. The net upward shortwave flux increased substantially in the sea ice variability region in the Okhotsk Sea and decreased significantly in the western subarctic Pacific during the heavy ice years (Fig. 6b). The former increase reached 50 W m^{-2} and was primarily driven by the difference in albedo between sea ice and open water, since the downward shortwave flux increased by 10–20 W m^{-2} (Fig. 6d) because of the cloud cover reduction (Figs. 5a–c). The latter decrease in the net upward shortwave flux was mainly caused by the difference in the downward shortwave flux. The downward flux difference reached 20 W m^{-2} in the western subarctic (Fig. 6d), and its distribution was consistent with the changes in cloud cover (Figs. 5a–c).

The combined net upward long- and shortwave radiation fluxes largely offset each other, particularly in the North Pacific and the northern Okhotsk Sea (Figs. 6a,b). The sum of these fluxes ranged over 15–35 W m^{-2} in the central to southern Okhotsk Sea and 5–15 W m^{-2} in the North Pacific region with significant differences. Thus, the impact of the radiation heat flux difference was minor compared to that of the turbulent heat flux difference.

5. Storm track

Notably, the Pacific storm track exhibited differences between the heavy and light ice years (Fig. 7). Storm track activity is measured here by the February mean of meridional eddy heat flux ($\overline{T'v'}$) at 500 hPa (e.g., Nakamura et al. 2002), where T' and v' are the deviations of temperature and northward wind components from the 8-day running mean, respectively, and the overbar denotes the monthly mean. The results are qualitatively similar to $\overline{T'v'}$ at 850 hPa and to eddy kinetic energy at 500 and 850 hPa.

The storm track activity was weaker and extended zonally during the heavy ice years (Fig. 7a), whereas it was stronger and extended to the northeast during the light ice years (Fig. 7b). Significant differences were found in the northern Okhotsk Sea, east of the Kuril Islands, and in the western Bering Sea (stippling in Fig. 7c), suggesting possible influence of differences in surface heat flux or surface baroclinicity due to the SIA difference. Comparing with the empirical orthogonal functions of the storm track (Lau 1988), the storm track (Fig. 7) appeared to be formed by positive first and negative second modes in the heavy ice years and negative first and positive second modes in the light ice years, where the first and second modes represent the strength and meridional shift over the central and eastern Pacific, respectively. In terms of the cyclone density cluster by Sickmöller et al. (2000), the storm track in the

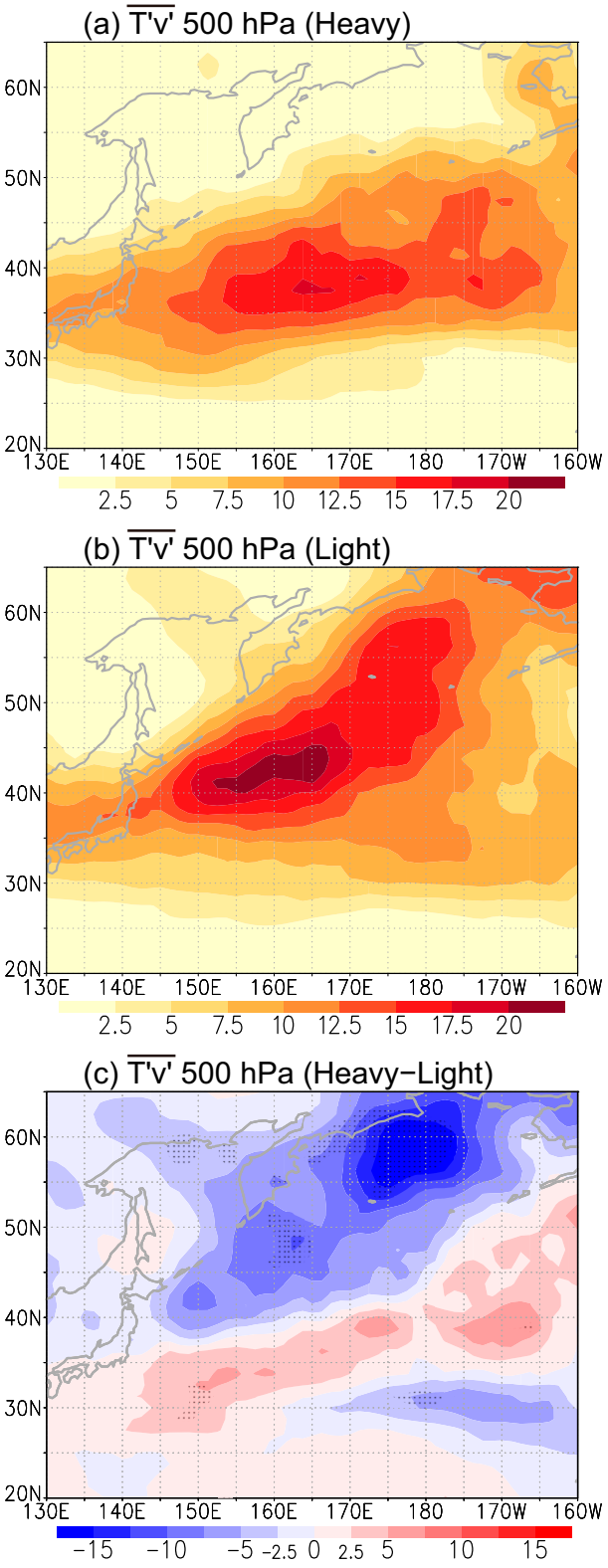

FIG. 7. Composites of storm track activity ($\overline{T'v'}$; K m s^{-1}) at 500 hPa during February in (a) heavy and (b) light ice years, and (c) the difference. Stippling in (c) denotes differences at 95% confidence level.

heavy and light ice years resembled zonal and northeastward clusters, respectively.

However, storm track variability is related to various factors, such as the monsoon, atmospheric teleconnections, snow cover, SST, SIA in the Bering Sea and Arctic, and feedback from disturbances (e.g., Overland and Pease 1982; Hoskins and Valdes 1990; Clark and Serreze 2000; Nakamura et al. 2002, 2004; Taguchi et al. 2009). These factors, especially the interannual variability of the background atmosphere, likely contributed to the above difference in the storm track. Although it is difficult for the present analysis method to separate the effects of SIA variation on the storm track and vice versa, the aforementioned results suggest a possibility that SIA in the Okhotsk Sea is one of the components of the storm track system.

6. Ocean mixed layer

The variations in surface heat flux would also influence the ocean. This section explores the differences in SST, sea surface density (SSD), and oceanic MLD in February, which are affected directly by the surface heat flux.

a. *Sea surface temperature and density*

SST was significantly lower (0.5°–1.5°C) in the Okhotsk Sea and the western subarctic Pacific during the heavy ice years (Fig. 8a). The distribution of the SST decrease resembled that of the decrease in SAT and the increase in the upward turbulent heat flux (Figs. 2c,a), suggesting the influence of cold and dry air advection. Although Nakanowatari et al. (2010) reported a negative correlation between SIA in the Okhotsk Sea and autumn SST in the East Kamchatka Current region, this correlation weakens in January. Indeed, the simple estimate in section 6b suggests that the difference in the surface heat flux contributed substantially to the significant SST decrease in the western subarctic Pacific in February.

SSD increased by 0.1–0.2 kg m^{-3} during the heavy ice years (Fig. 8b), corresponding mainly to the SST decrease (Fig. 8a). Consequently, denser water was entrained into the surface layer from below during heavy ice years, affecting nutrient circulation and primary production. In a region where SSD increase did not match SST decrease, it was associated with salinity increase, as SSD depends only on SST and salinity. This occurred around east of Sakhalin, the northern coast of the Okhotsk Sea, and the continental slope of the western Bering Sea. In particular, the increase in SSD east of Sakhalin was related to a decrease in sea surface salinity during the light ice years along the course of low-salinity water originating from the Amur River, consistent with the findings of Ogi and Tachibana (2006).

b. *Ocean mixed layer depth*

The ocean surface mixed layer was significantly deeper by 20–80 m in the North Pacific and in the southeastern and western parts of the Okhotsk Sea during the heavy-ice years (Fig. 8c). The MLD increase in the Pacific occurred in around 40°–45°N, corresponding to the salinity front along the subarctic-subtropical gyre boundary zone. Interestingly, this MLD increase in the Pacific occurred south (and partly in the southern part) of the regions with statistically significant differences in SST (Fig. 8a) and SSD (Fig. 8b) due to salinity stratification. Salinity governs the density stratification in the subarctic Pacific, a characteristic feature seen both in observations and the reanalysis. This strong salinity stratification (halocline) hinders the MLD increase caused by surface cooling. In the gyre boundary zone, a weak halocline allows for the mixed layer to deepen by surface cooling. North of the zone, MLD was barely increased by the SST decrease due to the strong halocline, with some contribution from pycnocline heaving associated with circulation change (not shown). The MLD difference was small south of the zone because of the minimal change in surface heat flux. In addition, the above difference in mixed layer development acts to enhance the difference between the distributions of MLD increase and SST decrease because mixed layer deepening increases its heat capacity.

Similar to the subarctic, the MLD increase due to SST decrease was also limited by the halocline in the Okhotsk Sea. The MLD increase in the western part was mostly associated with the decrease in salinity during the light ice years. The increase in the southeastern region was related to changes in both temperature and salinity.

To assess the extent of the MLD increase in the Pacific attributable to changes in the surface heat flux, a simple estimate was conducted. The estimate was based on a comparison between changes in the surface heat flux and mixed layer heat content in a region of significant MLD increase (40°–45°N, 155°–160°E). The area-averaged turbulent heat flux difference was ~80 W m^{-2}. The change in average radiation flux was small (~8 W m^{-2}) in the corresponding region. MLD in the heavy ice years ranged from 80 to 180 m, and mixed layer temperature was lower by 0.8°–1°C than in the light ice years. Consequently, in February, the change in surface turbulent heat flux accounted for 40%–50% of the change in the mixed layer heat content. The rest would be caused by the interannual variability in the background atmosphere and ocean. The above estimate suggests that heat flux variability related to SIA variability in the Okhotsk Sea makes a measurable contribution to MLD variability in the gyre boundary region.

7. Summary and discussion

Variations in SIA drastically alter the local heat exchange between the atmosphere and the ocean. The advection of less (more) heated air over large (small) SIA can enhance (reduce) the heat exchange downwind. The present study suggests that this is particularly effective for the Okhotsk Sea, located along the Asian winter monsoon route, and highlights the following possible impacts of interannual variability of SIA in the Okhotsk Sea on the downwind atmosphere and ocean:

1) The upward surface turbulent heat flux increased significantly in a broad region of the western North Pacific during the heavy ice years, downwind of a strong decrease in the heat flux over the sea ice variability region in the Okhotsk Sea. SAT and SH decreased over the sea ice variability region and its downwind approximately along the climatological winds. These distributions suggest the effect of Okhotsk Sea SIA variation; cold and dry air masses

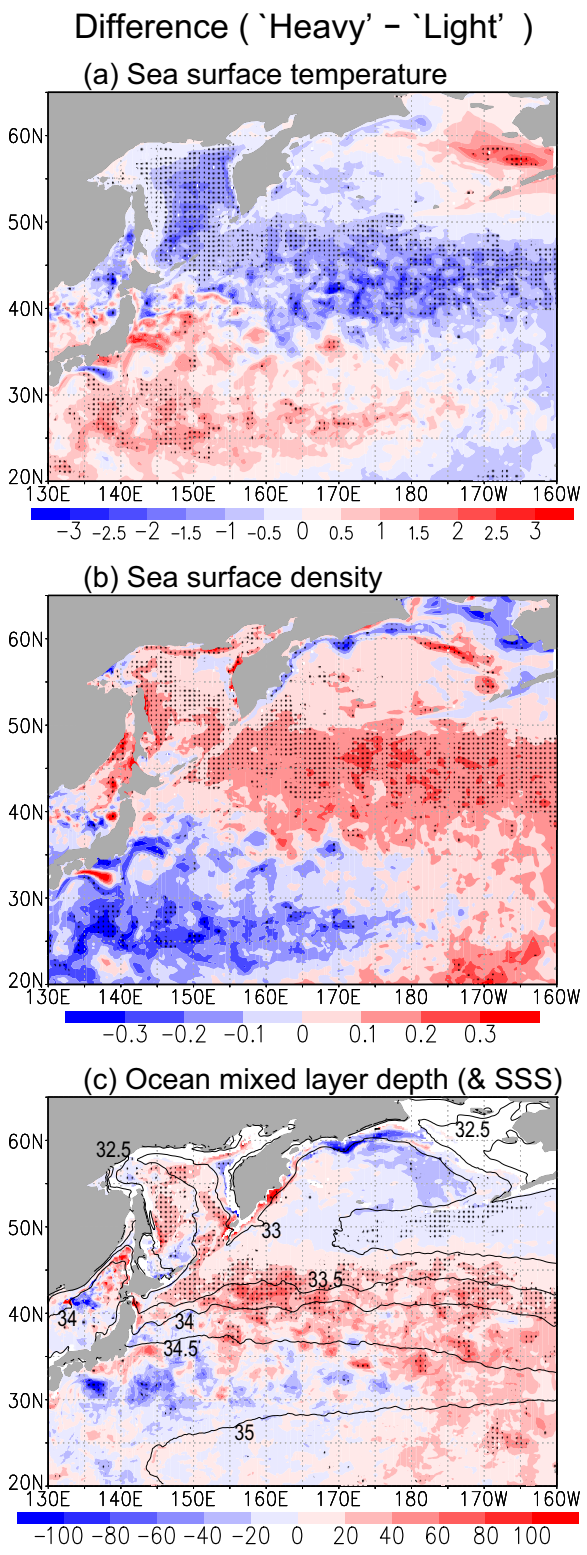

FIG. 8. Difference in (a) sea surface temperature (°C), (b) sea surface density (kg m^{-3}), and (c) ocean mixed layer depth (m) during February. Positive values indicate a relative increase in the heavy ice years. Climatological sea surface salinity contours are overlaid in (c). Stippling denotes differences at the 95% confidence level.

blowing from the Eurasian continent are exposed to less heating and moistening over a broader sea ice cover during heavy ice years, spreading farther downwind before modification. A simple estimate suggests that a major portion of the heat flux increase was associated with the SIA variation.

2) The surface longwave and shortwave radiation heat flux also varied significantly and was associated with differences in cloud cover, air temperature, effective water vapor amount, and albedo, although these fluxes largely offset each other.
3) The Pacific storm track differed in the heavy and light ice years; however, the effects of SIA on the storm track are unclear.
4) SST and ocean MLD varied significantly in the North Pacific and the Okhotsk Sea, although salinity stratification reduced MLD change in the subarctic. An estimate suggests that approximately half of the change in MLD was caused by a surface heat flux change in February in the North Pacific.

Notably, a region of significant heat flux change includes the Isoguchi jets or Oyashio Extension. Interannual SST variability in this region due to the meridional shift of the jets (~1°C) can affect North America and western Europe through teleconnections (Frankignoul et al. 2011) and the Pacific storm track (Smirnov et al. 2015). The differences in SAT and SST related to SIA variability in the Okhotsk Sea reached 2–4 K and 0.8°–1°C in the corresponding region. As these variabilities are much larger than and comparable to the above SST variability, these could affect the above atmospheric responses to SST variability.

Also, the total upward surface heat flux was larger in the heavy-ice years, despite the broader ice cover. Although part of this could be due to differences in the background atmosphere, feedback from the SIA variability may also play a role. For example, a broader ice cover enables cold and dry air to reach farther south, where the air contacts a higher SST, resulting in a larger heat flux.

Note that the present analysis did not isolate the effects of SIA variability. Separation of the effects of various factors is desired using an atmospheric general circulation model or an atmosphere–ocean coupled model. In particular, the variability of the Pacific storm track and the Okhotsk Sea SIA itself are considered to be associated strongly with the interannual variabilities of the atmosphere. Nevertheless, the calculated correlations were weak and complex between the meridional shift of the eastern part of the storm track and major atmospheric indices (including the Okhotsk SIA), such as the Pacific–North American (PNA) pattern, Aleutian low [North Pacific Index (NPI)], Arctic Oscillation (AO), western Pacific (WP) pattern, Pacific decadal oscillation, El Niño and Southern Oscillation [Niño-3 (NINO_west)], and the winter Asian monsoon (Winter Monsoon Index). Although the shift in the storm track was correlated with the PNA index and NPI in some instances, arguing for these correlations is challenging, considering the stringency of the significance test for multiple comparisons. Similarly, the correlations of SIA in the Okhotsk Sea with the above atmospheric indices were complex and inconclusive. Only the NPI was significant at a 95% confidence level. The AO index was significant only when the heavy and light ice

years were considered. Interestingly, when the years before 2002 were used to reduce the effects of global warming, the composites of SAT and SLP exhibited a WP-like structure, although the correlations with the above indices were insignificant. Nonetheless, these issues are difficult to resolve due to the problem of multiple comparisons.

The extensive impact of sea ice suggested in this study implies possible effects of the expected decrease due to global warming and the importance of sea ice in numerical modeling. The future SIA decrease would cause changes in 1) surface turbulent and radiation heat fluxes, air temperature, water vapor, and cloud cover from the Okhotsk Sea to the western subarctic and the boundary zone of the subarctic and subtropical gyres in the North Pacific, and 2) SST and MLD of the ocean in a similar region. Its influence could reach North America and Europe through atmospheric teleconnections. Associated changes in the MLD could affect ocean material circulation and ecosystems through wintertime nutrient supply from the subsurface, as well as water mass structure and circulation through mode water formation. Moreover, the present results suggest the importance of accurate sea ice reproduction in climate model simulations and realistic sea ice settings in atmospheric models (e.g., the effects of sea ice fraction and thickness). Nevertheless, the responses to sea ice loss in the future could be different from those in the past; if sea ice loss occurred concurrently around the Arctic, it may change the background atmosphere (Smith et al. 2022) and alter the responses to regional ice variations (Screen 2017). This is also left for future research.

Acknowledgments. This study was supported by JSPS KAKENHI (grants JP26247076, JP17H0115608, JP21K03655, and JP21H01154). The analysis was conducted using the Pan-Okhotsk Information System at Hokkaido University. The GrADS software was employed for generating figures and performing analyses. We express our gratitude to JAMSTEC and MRI for permission to use their FORA-WNP30 ocean reanalysis. We appreciate the three anonymous reviewers and an editor for their constructive comments and also thank Editage for language editing. To the best of our knowledge, there is no conflict of interest.

Data availability statement. The JRA-55 (https://jra.kishou.go.jp/JRA-55/index_en.html) and JMA sea ice extent (http://www.data.jma.go.jp/kaiyou/data/db/seaice/okhotsk/data/okhotsk_alldata.txt) data can be accessed online. The FORA-WNP30 dataset is available for research through JAMSTEC (https://search.diasjp.net/en/dataset/FORA_WNP30_JAMSTEC_MRI).

REFERENCES

Clark, M. P., and M. C. Serreze, 2000: Effects of variations in East Asian snow cover on modulating atmospheric circulation over the North Pacific Ocean. *J. Climate*, **13**, 3700–3710, https://doi.org/10.1175/1520-0442(2000)013<3700:EOVIEA>2.0.CO;2.

Deser, C., R. Tomas, M. Alexander, and D. Lawrence, 2010: The seasonal atmospheric response to projected Arctic sea ice loss in the late twenty-first century. *J. Climate*, **23**, 333–351, https://doi.org/10.1175/2009JCLI3053.1.

Fang, Z., and J. M. Wallace, 1994: Arctic sea ice variability on a timescale of weeks and its relation to atmospheric forcing. *J. Climate*, **7**, 1897–1914, https://doi.org/10.1175/1520-0442(1994)007<1897:ASIVOA>2.0.CO;2.

——, and ——, 1998: North-Pacific sea ice and Kuroshio SST variability and its relation to the winter monsoon. *Polar Meteor. Glaciol.*, **12**, 58–67, https://doi.org/10.15094/00002867.

Frankignoul, C., N. Sennéchael, Y.-O. Kwon, and M. A. Alexander, 2011: Influence of the meridional shifts of the Kuroshio and the Oyashio Extensions on the atmospheric circulation. *J. Climate*, **24**, 762–777, https://doi.org/10.1175/2010JCLI3731.1.

Honda, M., K. Yamazaki, H. Nakamura, and K. Takeuchi, 1999: Dynamic and thermodynamic characteristics of atmospheric response to anomalous sea-ice extent in the Sea of Okhotsk. *J. Climate*, **12**, 3347–3358, https://doi.org/10.1175/1520-0442(1999)012<3347:DATCOA>2.0.CO;2.

Hoskins, B. J., and P. J. Valdes, 1990: On the existence of storm-tracks. *J. Atmos. Sci.*, **47**, 1854–1864, https://doi.org/10.1175/1520-0469(1990)047<1854:OTEOST>2.0.CO;2.

Inoue, J., J. Ono, Y. Tachibana, M. Honda, K. Iwamoto, Y. Fujiyoshi, and K. Takeuchi, 2003: Characteristics of heat transfer over the ice covered Sea of Okhotsk during cold-air outbreaks. *J. Meteor. Soc. Japan*, **81**, 1057–1067, https://doi.org/10.2151/jmsj.81.1057.

Iwamoto, K., 2007: Heat budget in the Sea of Okhotsk based on rawinsonde observations (in Japanese). Meteorological Research Note 214, 19–26.

Japan Meteorological Agency, 2023: Sea ice in the Sea of Okhotsk. Last accessed 20 July 2023, https://www.data.jma.go.jp/kaiyou/data/shindan/a_1/series_okhotsk/longterm_okhotsk_latest.txt.

Katayama, A., 1966: On the radiation budget of the troposphere over the Northern Hemisphere (I). *J. Meteor. Soc. Japan*, **44**, 381–401, https://doi.org/10.2151/jmsj1965.44.6_381.

Kobayashi, S., and Coauthors, 2015: The JRA-55 reanalysis: General specifications and basic characteristics. *J. Meteor. Soc. Japan*, **93**, 5–48, https://doi.org/10.2151/jmsj.2015-001.

Kondo, J., 1975: Air-sea bulk transfer coefficients in diabatic conditions. *Bound.-Layer Meteor.*, **9**, 91–112, https://doi.org/10.1007/BF00232256.

——, 2000: *Atmospheric Science near the Ground Surface* (in Japanese). University of Tokyo Press, 324 pp.

Lau, N.-C., 1988: Variability of the observed midlatitude storm tracks in relation to low-frequency changes in the circulation pattern. *J. Atmos. Sci.*, **45**, 2718–2743, https://doi.org/10.1175/1520-0469(1988)045<2718:VOTOMS>2.0.CO;2.

Levitus, S., 1982: *Climatological Atlas of the World Ocean*. NOAA Prof. Paper 13, 173 pp. and 17 microfiche.

Liu, J., Z. Zhang, R. M. Horton, C. Wang, and X. Ren, 2007: Variability of North Pacific sea ice and East Asia–North Pacific winter climate. *J. Climate*, **20**, 1991–2001, https://doi.org/10.1175/JCLI4105.1.

Nakamura, H., T. Izumi, and T. Sampe, 2002: Interannual and decadal modulations recently observed in the Pacific storm track activity and East Asian winter monsoon. *J. Climate*, **15**, 1855–1874, https://doi.org/10.1175/1520-0442(2002)015%3C1855:IADMRO%3E2.0.CO;2.

——, T. Sampe, Y. Tanimoto, and A. Shimpo, 2004: Observed associations among storm tracks, jet streams and midlatitude oceanic fronts. *Earth's Climate: The Ocean-Atmosphere Interaction*, *Geophys. Monogr.*, Vol. 147, Amer. Geophys. Union, 329–345, https://doi.org/10.1029/147GM18.

Nakanowatari, T., K. I. Ohshima, and S. Nagai, 2010: What determines the maximum sea ice extent in the Sea of Okhotsk? Importance of ocean thermal condition from the Pacific. *J. Geophys. Res.*, **115**, C12031, https://doi.org/10.1029/2009JC006070.

Nihashi, S., K. I. Ohshima, and N. Kimura, 2012: Creation of a heat and salt flux dataset associated with sea ice production and melting in the Sea of Okhotsk. *J. Climate*, **25**, 2261–2278, https://doi.org/10.1175/JCLI-D-11-00022.1.

Ogi, M., and Y. Tachibana, 2006: Influence of the annual Arctic Oscillation on the negative correlation between Okhotsk Sea ice and Amur River discharge. *Geophys. Res. Lett.*, **33**, L08709, https://doi.org/10.1029/2006GL025838.

Ohshima, K. I., T. Watanabe, and S. Nihashi, 2003: Surface heat budget of the sea of Okhotsk during 1987–2001 and the role of sea ice on it. *J. Meteor. Soc. Japan*, **81**, 653–677, https://doi.org/10.2151/jmsj.81.653.

——, S. Nihashi, E. Hashiya, and T. Watanabe, 2006: Interannual variability of sea ice area in the sea of Okhotsk: Importance of surface heat flux in fall. *J. Meteor. Soc. Japan*, **84**, 907–919, https://doi.org/10.2151/jmsj.84.907.

Overland, J. E., and C. H. Pease, 1982: Cyclone climatology of the Bering Sea and its relation to sea ice extent. *Mon. Wea. Rev.*, **110**, 5–13, https://doi.org/10.1175/1520-0493(1982)110<0005:CCOTBS>2.0.CO;2.

Parkinson, C. L., and D. J. Cavalieri, 2008: Arctic sea ice variability and trends, 1979–2006. *J. Geophys. Res.*, **113**, C07003, https://doi.org/10.1029/2007JC004558.

Sasaki, Y. N., Y. Katagiri, S. Minobe, and I. G. Rigor, 2007: Autumn atmospheric preconditioning for interannual variability of wintertime sea-ice in the Okhotsk Sea. *J. Oceanogr.*, **63**, 255–265, https://doi.org/10.1007/s10872-007-0026-5.

Screen, J. A., 2017: Simulated atmospheric response to regional and pan-Arctic sea ice loss. *J. Climate*, **30**, 3945–3962, https://doi.org/10.1175/JCLI-D-16-0197.1.

Sickmöller, M., R. Blender, and K. Fraedrich, 2000: Observed winter cyclone tracks in the Northern Hemisphere in re-analysed ECMWF data. *Quart. J. Roy. Meteor. Soc.*, **126**, 591–620, https://doi.org/10.1002/qj.49712656311.

Smirnov, D., M. Newman, M. A. Alexander, Y.-O. Kwon, and C. Frankignoul, 2015: Investigating the local atmospheric response to a realistic shift in the Oyashio sea surface temperature front. *J. Climate*, **28**, 1126–1147, https://doi.org/10.1175/JCLI-D-14-00285.1.

Smith, D. M., and Coauthors, 2022: Robust but weak winter atmospheric circulation response to future Arctic sea ice loss. *Nat. Commun.*, **13**, 727, https://doi.org/10.1038/s41467-022-28283-y.

Tachibana, Y., M. Honda, and K. Takeuchi, 1996: The abrupt decrease of the sea ice over the southern part of the Sea of Okhotsk in 1989 and its relation to the recent weakening of the Aleutian low. *J. Meteor. Soc. Japan*, **74**, 579–584, https://doi.org/10.2151/jmsj1965.74.4_579.

Taguchi, B., H. Nakamura, M. Nonaka, and S. Xie, 2009: Influences of the Kuroshio/Oyashio Extensions on air-sea heat exchanges and storm-track activity as revealed in regional atmospheric model simulations for the 2003/04 cold season. *J. Climate*, **22**, 6536–6560, https://doi.org/10.1175/2009JCLI2910.1.

Thomson, R. E., and I. V. Fine, 2003: Estimating mixed layer depth from oceanic profile data. *J. Atmos. Oceanic Technol.*, **20**, 319–329, https://doi.org/10.1175/1520-0426(2003)020<0319:EMLDFO>2.0.CO;2.

Ukita, J., M. Honda, H. Nakamura, Y. Tachibana, D. J. Cavalieri, C. L. Parkinson, H. Koide, and K. Yamamoto, 2007: Northern Hemisphere sea ice variability: Lag structure and its implications. *Tellus*, **59A**, 261–272, https://doi.org/10.1111/j.1600-0870.2006.00223.x.

Usui, N., and Coauthors, 2017: Four-dimensional variational ocean reanalysis: A 30-year high-resolution dataset in the western North Pacific (FORA-WNP30). *J. Oceanogr.*, **73**, 205–233, https://doi.org/10.1007/s10872-016-0398-5.

Yamamoto, K., Y. Tachibana, M. Honda, and J. Ukita, 2006: Intraseasonal relationship between the Northern Hemisphere sea ice variability and the North Atlantic Oscillation. *Geophys. Res. Lett.*, **33**, L14711, https://doi.org/10.1029/2006GL026286.

Yamazaki, K., 2000: Interaction between the wintertime atmospheric circulation and the variation in the sea ice extent of the Sea of Okhotsk (in Japanese with English abstract). *Seppyo*, **62**, 345–354, https://doi.org/10.5331/seppyo.62.345.